Geochemistry Geophysics Geosystems G3

Article
Volume 13, Number 2
18 February 2012
Q02007, doi:10.1029/2011GC003881
ISSN: 1525-2027

Published by AGU and the Geochemical Society

Shear wave splitting at the Hawaiian hot spot from the PLUME land and ocean bottom seismometer deployments

John A. Collins
Department of Geology and Geophysics, Woods Hole Oceanographic Institution, Woods Hole, Massachusetts 02543, USA

Cecily J. Wolfe
Hawaii Institute of Geophysics and Planetology, University of Hawai'i at Mānoa, Honolulu, Hawaii 96822, USA (cecily@soest.hawaii.edu)

Department of Terrestrial Magnetism, Carnegie Institution of Washington, Washington, DC 20015, USA

Gabi Laske
Institute of Geophysics and Planetary Physics, University of California at San Diego, La Jolla, California 92093, USA

[1] We examine upper mantle anisotropy across the Hawaiian Swell by analyzing shear wave splitting of teleseismic *SKS* waves recorded by the PLUME broadband land and ocean bottom seismometer deployments. Mantle anisotropy beneath the oceans is often attributed to flow-induced lattice-preferred orientation of olivine. Splitting observations may reflect a combination of both fossil lithospheric anisotropy and anisotropy due to present-day asthenospheric flow, and here we address the question whether splitting provides diagnostic information on possible asthenospheric plume flow at Hawaii. We find that the splitting fast directions are coherent and predominantly parallel to the fossil spreading direction, suggesting that shear wave splitting dominantly reflects fossil lithospheric anisotropy. The signature of anisotropy from asthenospheric flow is more subtle, although it could add some perturbation to lithospheric splitting. The measured delay times are typically 1 s or less, although a few stations display larger splitting delays of 1–2 s. The variability in the delay times across the different stations indicates differences in the degree of anisotropy or in the thickness of the anisotropic layer or in the effect of multilayer anisotropy. Regions with smaller splitting times may have experienced processes that modified the lithosphere and partially erased the fossil anisotropy; alternatively, asthenospheric splitting may either constructively add to or destructively subtract from lithospheric splitting to produce the observed variability in delay times.

Components: 7600 words, 9 figures, 2 tables.

Keywords: Hawaii; splittting.

Index Terms: 7208 Seismology: Mantle (1212, 1213, 8124); 8121 Tectonophysics: Dynamics: convection currents, and mantle plumes; 8137 Tectonophysics: Hotspots, large igneous provinces, and flood basalt volcanism.

Received 20 September 2011; **Revised** 17 January 2012; **Accepted** 17 January 2012; **Published** 18 February 2012.

Collins, J. A., C. J. Wolfe, and G. Laske (2012), Shear wave splitting at the Hawaiian hot spot from the PLUME land and ocean bottom seismometer deployments, *Geochem. Geophys. Geosyst.*, *13*, Q02007, doi:10.1029/2011GC003881.

1. Introduction

[2] Hawaii has long been viewed as the archetypical hot spot. The Hawaiian-Emperor chain is located in an intraplate setting within the Pacific plate, records voluminous, age-progressive volcanism for >75 My [*Duncan and Keller*, 2004], and exhibits a broad topographic high known as the Hawaiian Swell [*Dietz and Menard*, 1953; *Crough*, 1978]. It has been proposed that a deep-rooted, high-temperature, upwelling mantle plume generates the Hawaiian hot spot [*Morgan*, 1971], and numerous numerical studies have been undertaken to assess the possible patterns of plume flow and melting in the mantle [e.g., *Davies*, 1988; *Sleep*, 1990; *Moore et al.*, 1998; *Ribe and Christensen*, 1999; *Farnetani and Hofmann*, 2010; *Ballmer et al.*, 2011]. Recent regional [*Wolfe et al.*, 2009, 2011] 3-dimensional seismic imaging at Hawaii has documented low seismic velocities extending from the upper mantle into the lower mantle, consistent with the existence of a high-temperature, upwelling mantle plume. The existence of anisotropy in the oceanic upper mantle is often attributed to strain-induced lattice-preferred orientation (LPO) of olivine *a* axes [100] [*Christensen*, 1984], with fast directions providing information on the direction of mantle flow in olivine aggregates for large deformations [*Zhang and Karato*, 1995]. However, the development of LPO may in some cases have a complex dependence on the finite strain history [*Kaminski and Ribe*, 2002]. Melt inclusions are another potential source of mantle anisotropy [*Blackman and Kendall*, 1997; *Jousselin and Mainprice*, 1998]. Thus the characterization of anisotropy may provide constraints on the pattern of upper mantle flow and melting at Hawaii.

[3] Shear wave splitting studies have been performed at several hot spot regions, including Iceland [*Bjarnason et al.*, 2002; *Xue and Allen*, 2005], Yellowstone [*Waite et al.*, 2005], the South Pacific superswell [*Fontaine et al.*, 2007], Galápagos [*Fontaine et al.*, 2005], Eiffel [*Walker et al.*, 2005a], and Hawaii [*Wolfe and Silver*, 1998; *Walker et al.*, 2001, 2003; *Collins et al.*, 2002]. One special focus of hot spot splitting investigations has been to ascertain whether the measured spatial distribution of anisotropy provides any diagnostic evidence of asthenospheric plume flow [*Rümpker and Silver*, 2000; *Walker et al.*, 2001, 2005b; *Waite et al.*, 2005].

[4] At Hawaii, it has been suggested that radial flow of plume material in the asthenosphere combined with shear in the absolute plate motion direction by the moving plate should produce a thick, coherent layer with asthenospheric plume flow that is parabolic in map view [*Sleep*, 1990]. *Walker et al.* [2001, 2003] attributed the splitting patterns around Hawaii to reflect a thick anisotropic layer with such plume-generated parabolic flow. However, their interpretation was severely limited by the sparse station coverage, since splitting measurements were only available at just 5 locations: on the island of Oahu (Global Seismic Network Station KIP), on the island of Hawaii (POHA), at the Ocean Seismic Network borehole station south of Oahu [*Collins et al.*, 2002], at the seafloor H2O site east of Hawaii [*Duennebier et al.*, 2002], and at Johnson atoll (JOHN). *Karato* [2008] also proposed another type of model where plume-asthenosphere interactions in the central Pacific and around Hawaii are a major influence on geophysical anomalies and anisotropy.

[5] Prior studies in the Pacific and around Hawaii have also suggested two potential layers of mantle anisotropy [see *Nishimura and Forsyth*, 1988, 1989; *Wolfe and Silver*, 1998]: a lithospheric layer with inherited anisotropy that was formed near the Pacific ridge axis [e.g., *Wolfe and Solomon*, 1998; *Harmon et al.*, 2004] with fast axis aligned parallel to the fossil spreading direction, and an asthenospheric layer, with anisotropic fast axis aligned parallel to the present-day mantle flow. Observations of mantle anisotropy at Hawaii thus also may be important for understanding the evolution of the lithosphere, as reflected in the degree of preservation of fossil anisotropy.

[6] The Plume-Lithosphere Undersea Melt Experiment (PLUME) project consisted of two one-yearlong deployments of ocean bottom seismographs (OBSs) and a concurrent land deployment, and provides an opportunity to assess the anisotropic mantle structure across a broad region around Hawaii. New splitting measurements from the PLUME seismometer deployments (Figure 1) provide unprecedented station coverage on the islands and the seafloor around Hawaii. Here we report shear wave splitting measurements at 49 sites, which dramatically improves the identification of splitting patterns, allowing us to reevaluate past interpretations regarding lithospheric and asthenospheric anisotropy across the Hawaiian Swell.

2. Shear Wave Splitting Analysis

[7] A shear wave passing through a single homogeneous anisotropic layer splits into two orthogonal

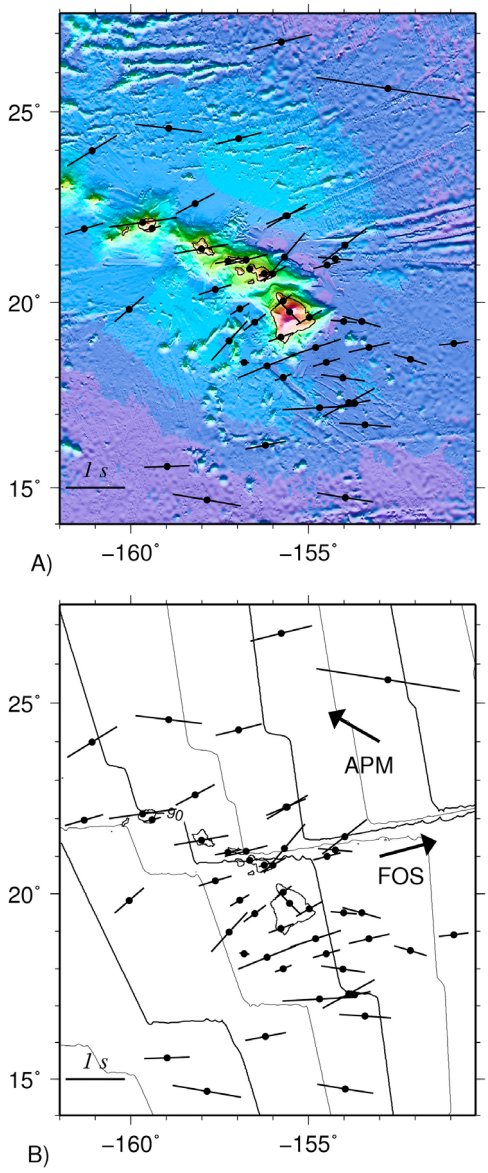

Figure 1. Splitting measurements on PLUME. (a) Plot of splitting measurements and bathymetry (from an updated version of *Smith and Sandwell* [1997]). Splitting delay time scale is provided in lower left corner. (b) Plot of splitting measurements and magnetic lineations [*Müller et al.*, 1997]. Arrows indicate the absolute plate motion direction (APM) from *Gripp and Gordon* [2002] and the fossil spreading direction (FOS). For a more detailed and accurate description of the Molokai Fracture Zone around Hawaii, see *Searle et al.* [1993].

waves with different wave speeds. Measurements of shear wave splitting constrain the fast shear wave polarization direction ϕ and the delay time δt between fast and slow shear waves. *SKS* waves undergo a *P*-to-*S* conversion at the core-mantle boundary, where they become radially polarized, so any observed anisotropy must come from the upgoing portion of the path between the core and receiver. *SKS* splitting parameters thus reflect the path-integrated effects of anisotropy beneath the receiving seismometer, and can provide information on the orientation of anisotropy as well as the combined effects of the thickness of the anisotropic layer, the degree of anisotropy, and the isotropic velocity [*Silver and Chan*, 1991].

[8] The PLUME project consisted of two one-yearlong deployments of ocean bottom seismographs in 2005–2006 and 2006–2007, as well as a concurrent deployment of land seismometers. Detailed information on the PLUME project can be found in the works of *Laske et al.* [2009] and *Leahy et al.* [2010] and the supporting online information of *Wolfe et al.* [2009]. High levels of seafloor noise on the horizontal components of the PLUME OBSs makes the measurement of shear wave splitting challenging. Microseismic noise limits the high-frequency end (>0.1 Hz) of the band where useful measurements can be made [e.g., *Collins et al.*, 2001]. Because the seismometer is deployed on the seafloor (rather than being buried), it is subject to seafloor-current induced tilting, which limits the lower end of the measurement band. At some PLUME stations, we typically observe *SKS* phases of sufficient quality for constraining splitting parameters in a narrow ~0.05–0.1 Hz frequency band, although other PLUME stations failed to provide any useful data for splitting.

[9] A general rule based on synthetic tests is that for single-event analyses, waveforms containing energy at periods less that 10 times the splitting delay δt are required to obtain a good measurement. The PLUME waveforms at 0.05–0.1 Hz, and with higher noise levels than at seismometers in continental interiors, are thus of borderline quality for obtaining individual splitting parameters when $\delta t \leq 1$ s. We therefore apply the multiple-event method of *Wolfe and Silver* [1998] for deriving optimum splitting parameters from *SKS* phases of multiple earthquakes, which significantly improves resolution of splitting parameters [see also *Restivo and Helffrich*, 1999; *Monteiller and Chevrot*, 2010], particularly when the events occur at differing backazimuths. This method analyzes waveforms from multiple events at a given station and determines the best pair of splitting parameters (ϕ, δt) that can explain the suite of events. We choose to best linearize horizontal particle motion, rather than to minimize transverse energy; both options are implemented in the codes of *Silver and Chan* [1991] and *Wolfe and Silver* [1998]. The former method will absorb any possible error in the OBS

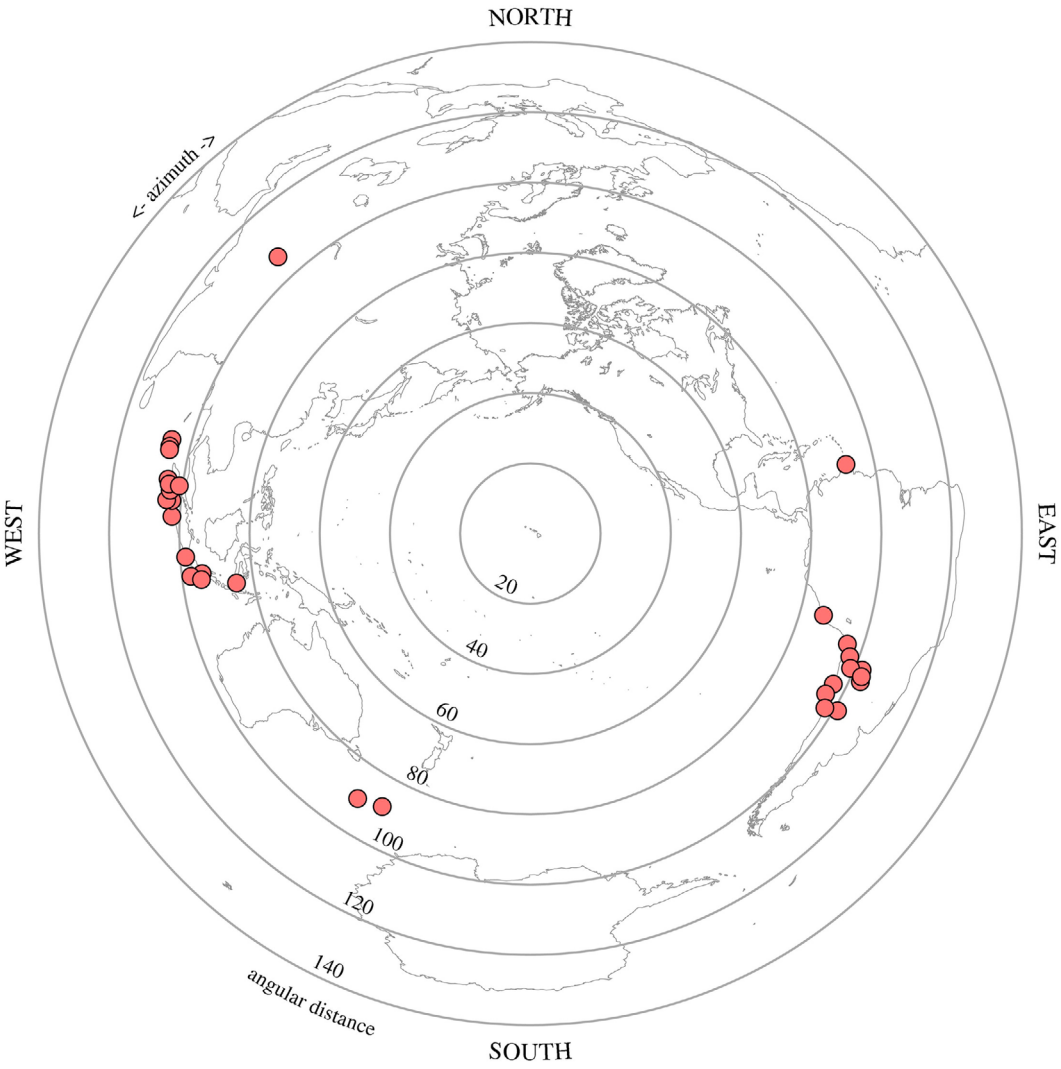

Figure 2. Earthquake epicenters used in the splitting analysis, with respect to Hawaii. Coastlines are indicated by gray lines.

horizontal-component orientations directly into ϕ without affecting δt. The horizontal orientations of OBSs were estimated from teleseismic P wave particle motion analyses and have errors of ~5°; PLUME land seismometer orientations are derived using a magnetic compass and should have smaller errors. The multiple event splitting method is designed for single layer anisotropy, although *Wolfe and Silver* [1998] show how it can be adapted to two-layer anisotropy if the back-azimuthal coverage of earthquakes is adequate.

[10] Teleseismic splitting analyses were designed for the case of a single anisotropic layer (representing the path-integrated anisotropy), which may amalgamate multiply split waves into a single apparent splitting parameter. It is more difficult to obtain information on depth-varying anisotropy. Several promising avenues for gaining further insight include two-layer splitting analyses [*Silver and Savage*, 1994], comparison of splitting with the predictions from numerical geodynamic models [e.g., *Blackman and Kendall*, 2002; *Kaminski and Ribe*, 2002; *Becker et al.*, 2006], combined interpretation with surface wave or P_n anisotropy [*Li and Detrick*, 2003; *Marone and Romanowicz*, 2007], or, if data coverage and quality is sufficient, splitting tomography [*Chevrot*, 2006; *Abt and Fischer*, 2008].

3. Shear Wave Splitting Results

[11] We examined *SKS* records at distances >85°–120° from earthquakes of moment magnitude (M_w) 5.5 or larger in the Global Centroid Moment Tensor

Table 1. Earthquakes Used in the Analyses

Year	Julian Day	Latitude (deg)	Longitude (deg)	Depth (km)	Mw	BAZ (deg)
2005	057	2.91	95.59	36	6.7	279
2005	080	−24.98	−63.47	579	6.9	113
2005	100	−1.64	99.61	19	6.7	273
2005	134	0.59	98.46	34	6.8	276
2005	164	−19.99	−69.20	116	7.8	110
2005	186	1.82	97.08	21	6.7	277
2005	205	7.92	92.19	16	7.3	285
2005	281	34.54	73.59	26	7.6	318
2005	321	−22.32	−67.89	163	6.8	111
2006	120	−27.01	−70.96	27	6.6	117
2006	136	0.09	97.05	12	6.8	275
2006	146	−7.96	110.45	12	6.4	264
2006	172	6.94	92.45	16	6.0	284
2006	178	6.50	92.79	28	6.2	284
2006	197	−28.72	−72.54	10	6.2	119
2006	198	−9.25	107.41	34	7.7	263
2006	200	−6.53	105.39	45	6.2	267
2006	208	1.71	97.15	20	6.2	277
2006	223	2.40	96.35	22	6.3	278
2006	237	−24.41	−67.03	184	6.6	113
2006	252	−7.21	120.11	572	6.3	261
2006	260	−31.75	−67.18	142	6.2	120
2006	264	−9.05	110.36	25	6.0	262
2006	265	−26.87	−63.15	598	6.0	115
2006	272	10.88	−61.76	53	6.1	78
2006	285	−31.30	−71.33	46	6.4	121
2006	293	−13.46	−76.68	23	6.7	106
2006	317	−26.04	−63.22	552	6.9	114
2006	320	−52.00	139.47	10	6.1	214
2006	335	3.40	99.09	205	6.3	278
2007	030	−54.74	146.3	11	6.9	209

Catalog. We find that almost all useable data are from larger earthquakes, generally $M_w \geq 6.5$ on PLUME OBS stations and $M_w \geq 6$ on PLUME land stations. The subset of waveforms used for splitting is also smaller than the subset of *SKS* phases that provided delay times for 3-dimensional imaging [*Wolfe et al.*, 2009], because splitting measurements require good signal-to-noise ratio on both the radial and the transverse components. We did not observe any clear *SKKS* phases on PLUME.

[12] The distribution of earthquake epicenters that provided useful data for splitting is displayed in Figure 2 and listed in Table 1. For assessing possible two-layer anisotropy, it is important to have a range of backazimuthal coverage. Unfortunately, as shown in Figure 2, our backazimuthal coverage is too limited to constrain two-layer anisotropic models. Most events come from the South American subduction zone to the southeast and the Sumatra subduction zone to the west. On the first PLUME deployment, *SKS* phases from the damaging M_w 7.6 Pakistan earthquake in 2005 were recorded with good signal-to-noise ratio on more than half of the stations, providing additional coverage from the northwest. A small number of stations on the second PLUME deployment also recorded good *SKS* phases from two events at the western Indian-Antarctic ridge with southern backazimuth and from an earthquake in Trinidad with eastern backazimuth.

[13] All measurements are carefully reviewed using the diagnostic plots of *Silver and Chan* [1991]. Clear splitting is present on some seismograms: prior to correcting for anisotropy, there is noticeable energy on the transverse component, elliptical particle motion, and when components are rotated into the fast and slow directions (not shown), two split *S* waves are evident. Correcting for splitting using the multiple-event solution removes these characteristics and linearizes particle motion. For the case of small or null splitting, across multiple events we systematically observe minimal energy on the transverse component and linear particle motion.

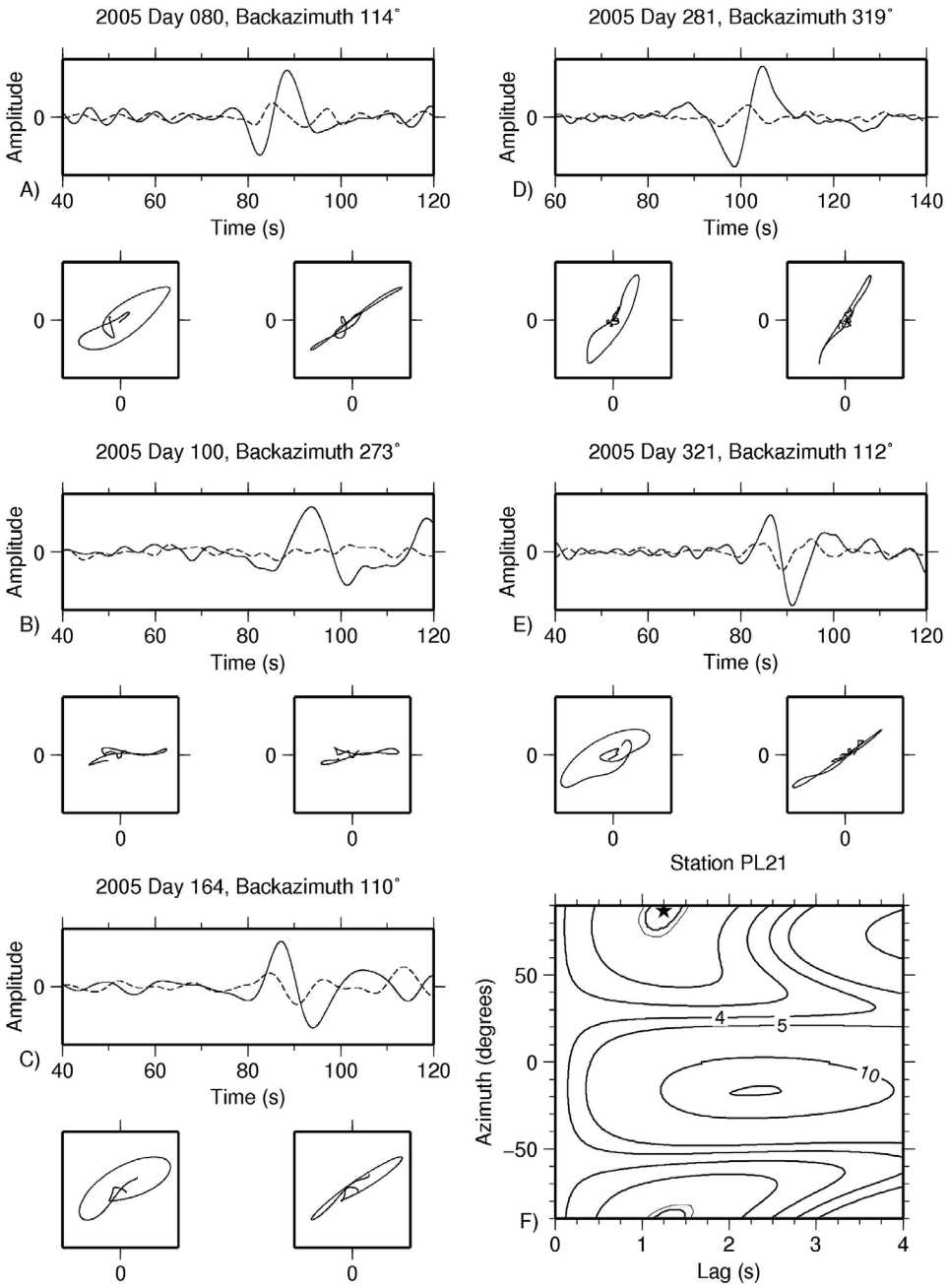

Figure 3. Splitting at OBS station PL21 from the first PLUME deployment, where several events display a high quality split shear wave on the transverse component. The solution (Figure 3e) is constrained by a set of 7 events. (a–e) Examples of data used for the analyses. (top) Radial (solid line) and transverse (dashed line) component *SKS* data from one earthquake. (bottom) Corresponding particle motion of *SKS* data in the fast-slow reference frame before (left) and after (right) correcting for the solution splitting parameters. Elliptical motion indicates splitting, whereas correcting for splitting linearizes particle motion. (e) Contour plot of stacked energy [*Wolfe and Silver*, 1998] on the solution transverse components as a function of the delay time δt and the polarization angle ϕ of the fast split shear wave. The double contour represents the 95% confidence interval, and the star indicates the best solution, which is well constrained.

[14] Because of strong differences in signal-to-noise levels, solution quality is highly variable from station to station. To illustrate the range of station quality, we provide example plots of splitting diagnostics in Figures 3–7. Figure 3 shows an example of waveforms on the first PLUME deployment from station PL21, where several earthquakes yield clear, high-quality records of

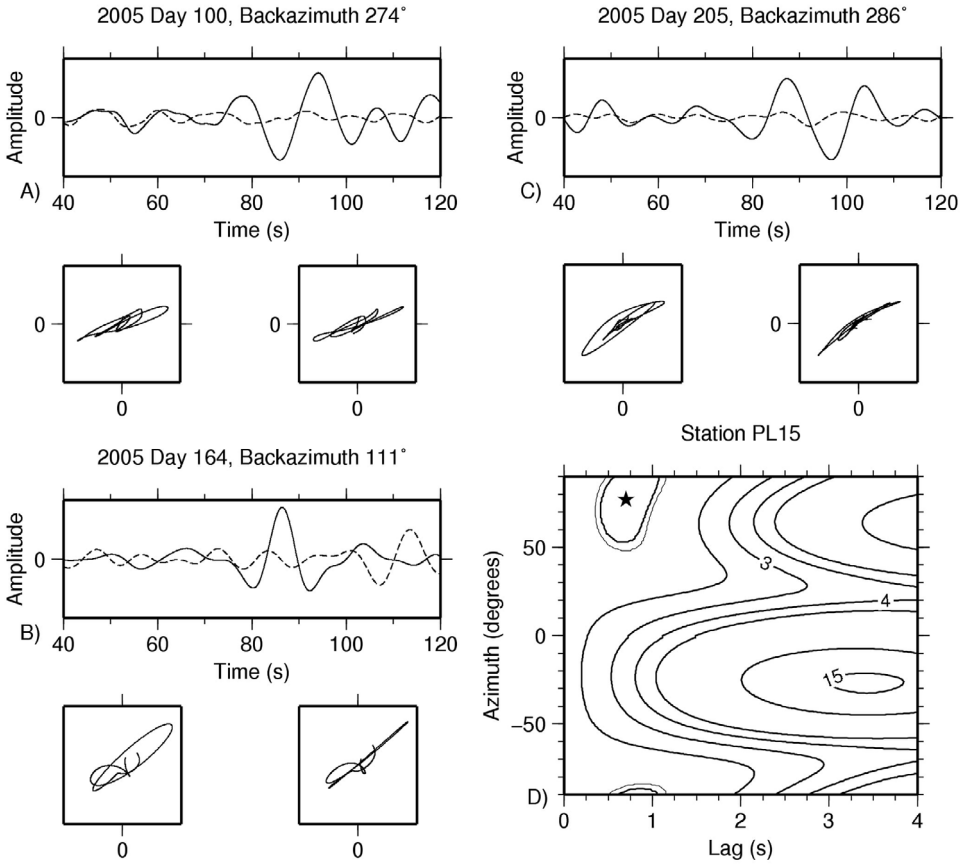

Figure 4. Splitting at OBS station PL15 from the first PLUME deployment, where splitting is subtle. The solution (Figure 4d) is constrained by 4 events. See Figure 3 for further information.

splitting. Splitting in this example is indicated by prominent arrivals on the transverse component at certain backazimuths (Figures 3a (top), 3d (top), and 3e (top)) and the elliptical particle motion (Figures 3a (bottom, left), 3d (bottom, left), and 3e (bottom, left)). The particle motion is linearized (Figures 3a (bottom, right), 3d (bottom, right), and 3e (bottom, right)) after correcting for splitting using the multiple-event solution, which is derived by analyzing the stacked energy on the solution transverse component as a function of splitting parameters (Figure 3f). Figure 4 shows the splitting analysis for station PL15 from the first PLUME deployment. On this station, *SKS* phases display more subtle splitting, but nonetheless, correcting for the multiple-event solution successfully linearizes the weakly elliptical particle motion. Figure 5 displays an example of diagnostics on one of the more quiet OBSs from the second PLUME deployment, and Figure 6 displays example diagnostics on one of the more noisy OBS from the second deployment. Finally, a very-well constrained null solution from station LHSM, on Maui, is displayed in Figure 7, where events from differing backazimuths display no splitting.

[15] Table 2 lists the splitting parameters at 49 stations, as well as the solution errors and the events that were used in the analyses. Delay times (δt) range from ~0 to 2.2 s and typical errors are $\pm 10°$ for ϕ and ± 0.2 s for δt. The results are plotted in Figures 1a and 1b. We note that the splitting method solves for the polarization of the *SKS* wave (after correcting for splitting). These polarizations are typically close to the backazimuth direction, with an overall residual standard deviation of 6° on OBSs, indicating that the horizontal components are well orientated.

4. Discussion

[16] The splitting measurements are displayed in Figure 1. The fast directions (ϕ) are coherent over a broad region and are predominantly parallel to the fossil spreading direction (~75°). For example, the

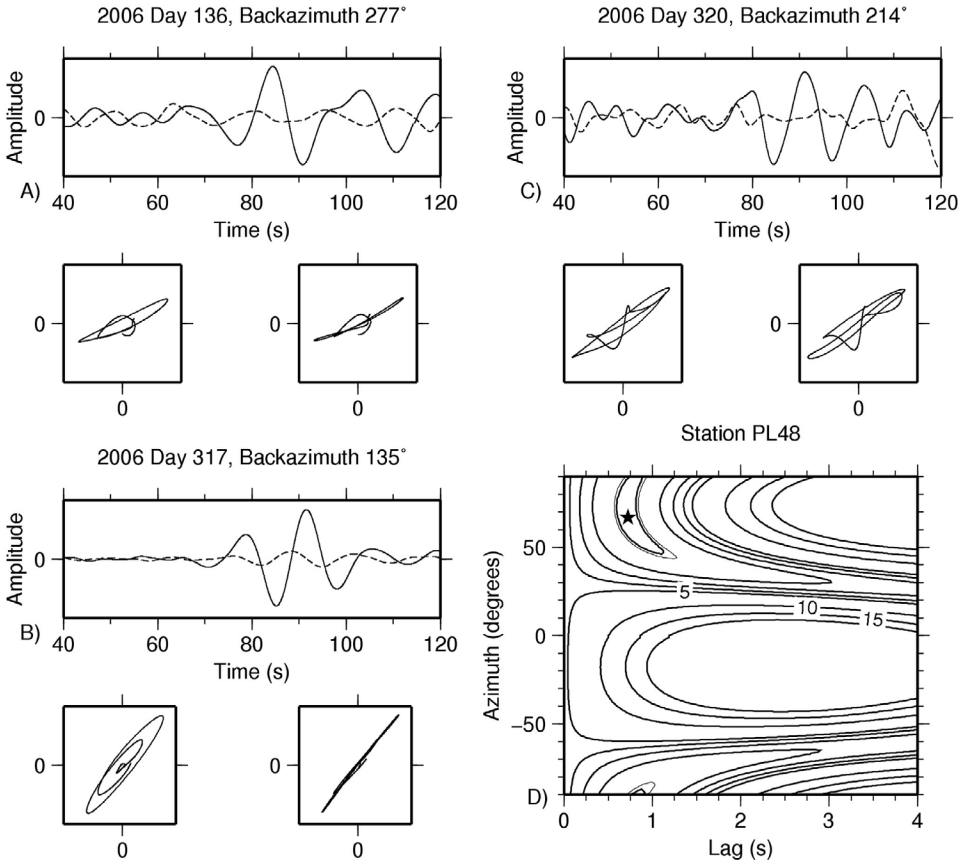

Figure 5. Splitting at OBS station PL48 from the second PLUME deployment, which is a quiet OBS station. The solution (Figure 5d) is constrained by a set of 4 events. See Figure 3 for further information.

mean value of all ϕ in Table 1 is 76°, although there is some variability in the directions, which have a standard deviation of 19°. Only one station, POHA on the island of Hawaii, exhibits splitting parallel to the absolute plate motion (APM) direction (−60°) [*Gripp and Gordon*, 2002]. Our results suggest that splitting dominantly reflects the fossil lithospheric anisotropy and that splitting from asthenospheric depths is less obvious. The fast directions around Hawaii do not yield the parabolic pattern predicted by some types of simple geodynamic models of flow and LPO development from a plume-fed asthenosphere (Figure 8), as was previously suggested by *Walker et al.* [2001, 2003] in their analyses with much more limited station coverage.

[17] Why does the splitting signal appear to be stronger from the lithosphere than from the asthenosphere? Several factors may explain the apparently weaker asthenospheric splitting. The first is if diffusion creep, which does not produce anisotropy, is the dominant deformation mechanism in the asthenosphere, rather than dislocation creep. However, this possibility seems unlikely, since a recent study of the shape of the Hawaiian swell supports a dislocation creep rheology in the asthenosphere [*Asaadi et al.*, 2011] and because surface wave studies indicate unusually strong (6%) radial anisotropy in the central and north Pacific at 100–200 km depth [*Ekström and Dziewoński*, 1998; *Nettles and Dziewoński*, 2008]. A second possibility is that the plume-fed asthenosphere could have less olivine and more clinopyroxene in the Hawaiian mantle source [*Sobolev et al.*, 2005]. The third possibility comes from studies such as *Karato et al.* [2008] and *Karato* [2008], where it is suggested that the mapping between mantle flow and anisotropy can be complex. Water content, temperature, and stress may alter the development and type of anisotropic olivine fabric, and *Karato* [2008] proposes a model whereby the plume-fed asthenosphere around Hawaii may have a fabric type yielding weaker splitting (but stronger radial anisotropy, consistent with surface wave studies).

[18] A fourth, and perhaps most promising, factor that may affect the splitting results is the presence of vertically varying anisotropic structure. Vertically varying flow in the asthenosphere occurs in

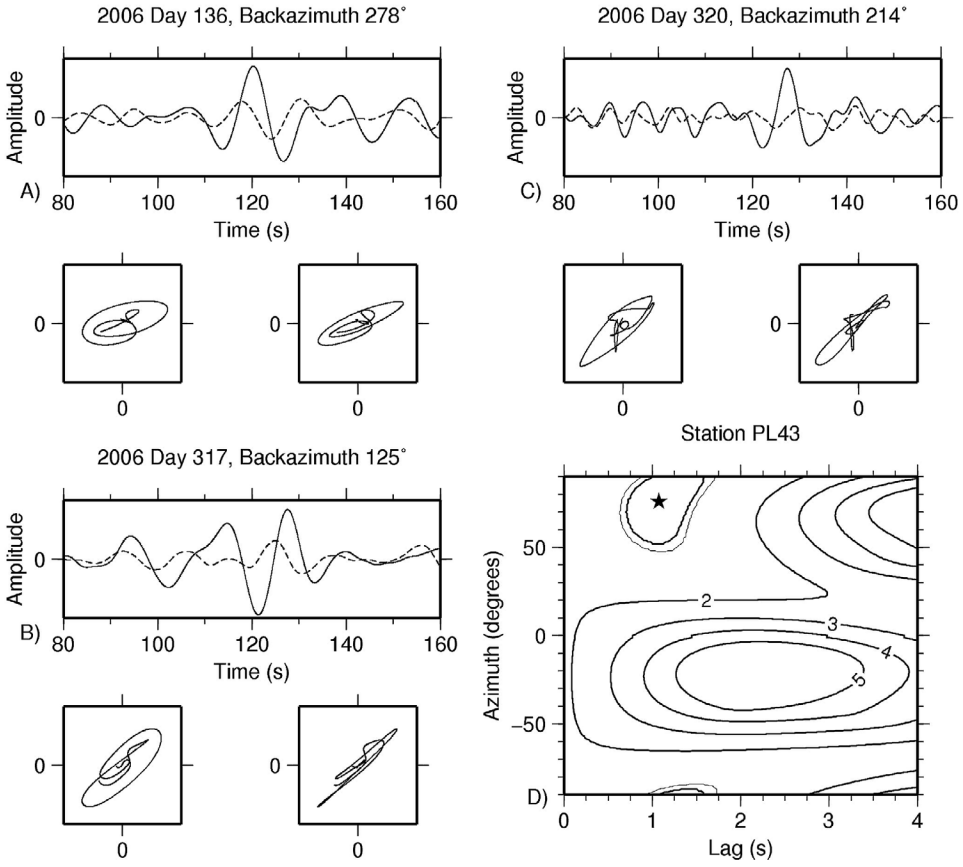

Figure 6. Splitting at OBS station PL43 from the second PLUME deployment. Note transverse component noise levels are higher at this station. The solution (Figure 6d) is constrained by a set of 5 events. See Figure 3 for further information.

some numerical Hawaiian plume models that include small-scale convection [*Moore et al.*, 1998; *Ballmer et al.*, 2011]; alternatively vertically varying anisotropic structure may reflect complexities in the mapping between mantle deformation and LPO. Flow in a plume-fed asthenosphere may generate fabric with varying orientation as a function of depth and fail to produce a thick and coherently orientated anisotropic layer that preserves a signature of parabolic flow. Strong vertical variations in the orientation of anisotropy can generate apparent small splitting from the relevant depth interval, as shown by *Rümpker and Silver* [1998] or *Saltzer et al.* [2000]. *Saltzer et al.* [2000] also suggest that splitting in heterogeneous media is more sensitive to the upper portions of the model, so if the orientation of anisotropy varies with depth, the splitting fast direction will be biased toward that of the topmost layer, thus potentially explaining the dominance of shallower lithospheric splitting at Hawaii.

[19] Future work should help narrow possible explanations. The study of Rayleigh wave azimuthal anisotropy from the PLUME project should contribute significantly by constraining the relative strength and direction of lithospheric and asthenospheric anisotropy: initial results [*Chojnacki et al.*, 2009] indicate Rayleigh wave fast directions oriented in the fossil spreading direction at frequencies of 30–50 mHz (corresponding to lithospheric depths), consistent with our inference that splitting patterns reflect fossil lithospheric anisotropy. This coherent pattern breaks down for lower frequencies, however, hinting at the presence of non-uniform anisotropy in the asthenosphere. Predictions of splitting from geodynamic models of plume flow and melting that incorporate LPO development using the method of *Kaminski and Ribe* [2002] should also be useful to assess the possible influence of vertically varying asthenospheric anisotropy. This method indicates that in regions where mantle flow varies over short length scales, interpreting anisotropy requires geodynamic models of mantle deformation and LPO, since LPO may not always parallel the mantle flow direction. A recent geodynamic study predicting

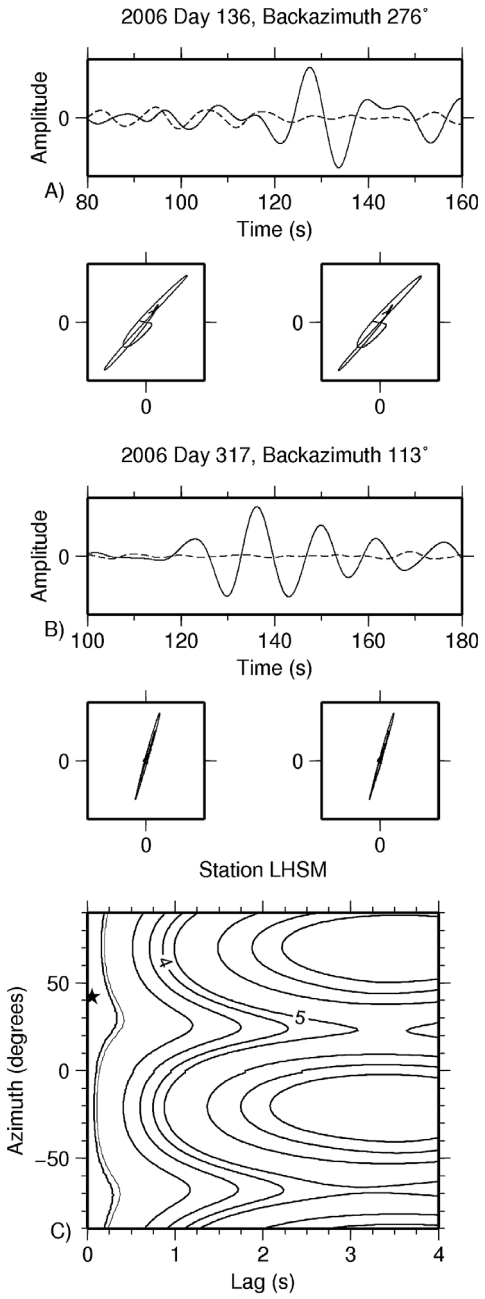

Figure 7. A well-constrained null splitting at land station LHSM on Maui. Note the lack of energy on the transverse components for differing backazimuths and the linear polarization. Contour plot (Figure 7c) of stacked energy [*Wolfe and Silver*, 1998] on the solution transverse components. The solution is constrained by a set of 6 events. See Figure 3 for further information.

splitting at Hawaii [*Ito et al.*, 2011] tests whether plume flow may add a recognizable perturbation to the dominantly lithospheric signal. Asthenospheric mantle flow (or melt) may either be oriented so that asthenospheric splitting constructively reinforces lithospheric splitting (when asthenospheric and lithospheric fast directions are parallel) or destructively decreases it (when asthenospheric and lithospheric fast directions are perpendicular). Thus the variability in splitting fast directions and delay times at Hawaii may reflect the influence of asthenospheric flow, rather than being due to variations in lithospheric anisotropy. If so, it may be possible to extract more information on asthenospheric anisotropy and plume flow by geodynamic modeling of these perturbations.

[20] Our measured delay times are typically 1 s or less, although a few stations display larger delay times of 1–2 s. Assuming a horizontal olivine *a*-axis and a single anisotropic layer, the variability in the delay times across the different stations indicates differences either in the degree of anisotropy or in the thickness of the anisotropic layer. Typical degrees of anisotropy from petrofabric measurements on mantle samples are 3–5% [*Mainprice and Silver*, 1993; *Silver et al.*, 1999], which yields about 1 s of splitting for a 100-km-thick anisotropic layer. The typical splitting times of 0.5–1 s in our study may therefore correspond to a 50 to 100 km thick anisotropic region.

[21] PLUME stations yielding small splitting times may alternatively reflect regions where processes have altered the lithosphere and erased some of the fossil anisotropy. Many of the locations with small delay times are on or near the Hawaiian Islands, where hot spot magma transport through the lithosphere may act to partially reduce the fossil lithospheric anisotropy. Weak splitting is observed on the islands of Maui and Hawaii, locations with high volcanic flux [*Van Ark and Lin*, 2004]. Magmatic underplating also occurs at the Hawaiian Islands [*Watts et al.*, 1985; *Leahy et al.*, 2010], and perhaps the lithosphere is modified by an extensive melt network with pathways that do not always reach the surface. There is also abundant mantle seismicity down to 50–60 km depth beneath the Island of Hawaii [*Wolfe et al.*, 2004], and faulting may perhaps be sufficiently pervasive to deform the lithosphere and partially erase the fossil anisotropy. Moreover, 3-dimensional imaging using PLUME surface wave data [*Laske et al.*, 2011] indicates decreased velocities beneath and around the islands at lithospheric and asthenospheric depths (40–140 km), also consistent with some level of modification of the fossil lithosphere.

[22] Figure 9 displays the splitting measurements superimposed on the average teleseismic *S* wave station delay times from *Wolfe et al.* [2009]. There is no simple linear relation between splitting delay

Table 2. PLUME Stations and Splitting Parameters

Station	Latitude	Longitude	Depth (m)	$\phi\pm$	$\delta t\pm$	Year/Day of Events (YY/JJJ)
BIG2	19.0790	−155.7730	582	70 ± 17	0.45 ± 0.17	05080, 05100, 05134, 05164, 05186, 06120, 06136, 06137
CCHM	20.7710	−155.9970	60	60 ± 14	0.5 ± 0.15	05080, 05164, 05281, 05321, 06136, 06317
DLAH	19.6010	−154.9830	52	61 ± 19	0.5 ± 0.17	05080, 05100, 05186, 05205, 06252, 06260, 06264
HPAH	20.0460	−155.7110	775	53 ± 19	0.35 ± 0.17	05080, 05100, 05281, 06120, 06136
KCCH	21.9710	−159.4010	128	75 ± 22	0.3 ± 0.4	05080, 05100, 05164, 05186, 05205, 05321, 06120, 06260, 06317, 06335
KIP	21.4233	−158.0150	37	80 ± 7	0.925 ± 0.15	05080, 05100, 05134, 06164, 05281, 05321
LHSM	20.8910	−156.6580	204	42 ± 22	0.05 ± 0.15	06120, 06136, 06252, 06260, 06317, 07030
MAUI	20.7668	−156.2448	2060	74 ± 22	0.2 ± 0.45	05080, 05100, 05164, 05186, 05281, 05321, 06120, 06136
MRKH	21.1090	−157.2700	143	79 ± 22	0.45 ± 0.47	05080, 05100, 05164, 05205, 06120, 06136
NGOK	22.1230	−159.6650	1157	82 ± 5	1.15 ± 0.17	06120, 06136, 06172, 06285, 06293, 06317, 06335, 07030
PHRM	21.1360	−156.7560	407	76 ± 12	0.74 ± 0.22	05080, 05164, 0581, 05321, 06120, 06136, 06172
POHA	19.7575	−155.5325	1966	−45 ± 10	0.55 ± 0.17	05281, 05321, 06136, 06260, 06265, 06285, 06317, 06335 07030, 07136
PL03	21.2055	−155.6794	−5144	40 ± 4	1.075 ± 0.17	05080, 05100, 05164, 05205, 05281, 05321
PL04	22.2936	−155.5947	−4515	60 ± 8	0.8 ± 0.12	05057, 05080, 05134, 05164, 05205, 05281
PL06	21.0000	−154.4828	−5373	76 ± 8	0.48 ± 0.11	05057, 05080, 05100, 05134, 05164, 05205, 05281
PL07	21.5197	−153.9827	−4912	52 ± 6	0.95 ± 0.0.25	050880, 05205, 05281, 05321
PL11	19.4952	−153.5032	−5181	−74 ± 20	0.675 ± 0.29	05080, 05164, 05205, 05281
PL12	19.5022	−154.0150	−5385	−85 ± 11	0.44 ± 0.14	05080, 05100, 05134, 05164, 05186, 05205, 05281, 05321
PL15	18.8009	−153.2959	−5077	77 ± 12	0.7 ± 0.16	05100, 05164, 05205, 05281
PL17	18.4814	−152.1324	−5184	−73 ± 22	0.575 ± 0.65	05080, 05164, 05205, 05281, 05321
PL19	16.7119	−153.4067	−5163	−86 ± 13	0.88 ± 0.28	05080, 05164, 05205, 05281, 05321
PL20	17.2975	−153.7008	−5120	79 ± 15	0.55 ± 0.2	05080, 05164, 05281, 05321
PL21	17.1803	−154.6925	−4993	87 ± 5	1.25 ± 0.11	05080, 05100, 05134, 05164, 05281, 05321
PL22	17.9884	−154.0305	−5057	−82 ± 7	0.75 ± 0.2	05057, 05164, 05205, 05281, 05321
PL23	18.4017	−154.4959	−5167	74 ± 9	0.475 ± 0.12	05080, 05100, 05281
PL24	18.8031	−154.7974	−5319	72 ± 14	0.9 ± 0.27	05080, 05164, 05281, 05321
PL27	18.0003	−155.7150	−5099	68 ± 19	0.3 ± 0.14	05080, 05100, 05134, 05164, 05205, 05281
PL29	18.4042	−156.8082	−4627	−84 ± 22	0.17 ± 0.39	05080, 05100, 05164, 05205, 05281, 05321
PL30	18.3010	−156.1670	−5091	68 ± 4	1.05 ± 0.16	05080, 05100, 05205, 05281, 05321
PL32	18.9831	−157.2286	−4604	42 ± 5	0.90 ± 0.13	05057, 05080, 05100, 05134, 05164, 05205, 05281
PL33	19.4777	−156.5101	−4707	53 ± 20	0.47 ± 0.24	05080, 05164, 05281, 05321
PL34	19.8327	−156.9320	−4748	59 ± 15	0.37 ± 0.12	05080, 05134, 05164, 05205, 05281, 05321
PL35	20.3461	−157.6276	−4650	73 ± 13	0.57 ± 0.17	05164, 05205, 05281, 05321
PL37	19.8234	−160.0475	−4676	49 ± 11	0.65 ± 0.17	06136, 06208, 06317
PL39	21.9563	−161.3149	−4543	74 ± 13	0.67 ± 0.19	06223, 06293, 06317, 06320, 06335
PL40	23.9931	−161.0931	−4691	58 ± 9	0.99 ± 0.14	06120, 06136, 06293, 06317, 07030
PL41	24.5738	−158.9331	−4749	−83 ± 7	1.12 ± 0.3	06120, 06223, 06260, 06293
PL43	26.7767	−155.7653	−5545	76 ± 22	1.07 ± 0.26	06136, 06200, 06260, 06317, 06320
PL44	25.5928	−152.7658	−5420	−81 ± 4	2.45 ± 0.31	06136, 06265, 06285, 06317
PL46	24.3121	−156.9646	−4428	76 ± 8	0.8 ± 0.1	06136, 06146, 06172, 06178, 06197, 06260, 06320
PL47	22.6217	−158.1842	−4830	62 ± 16	0.74 ± 0.25	06120, 06237, 06293, 06317, 07030
PL48	22.2999	−155.6362	−4528	67 ± 13	0.72 ± 0.21	06136, 06285, 06317, 06320
PL49	21.1669	−154.2492	−5173	−85 ± 15	0.58 ± 0.22	06198, 06260, 06317, 06335, 07030
PL57	18.9142	−150.9150	−5335	83 ± 22	0.50 ± 0.54	06136, 06237, 06285, 06317, 07030
PL63	14.7311	−153.9655	−5603	−81 ± 5	0.96 ± 0.19	06198, 06237, 06260, 06317
PL65	17.3154	−153.8682	−5115	61 ± 10	1.00 ± 0.12	06197, 06252, 06223, 06260, 06272, 06285
PL67	16.1630	−156.2070	−5112	79 ± 14	0.70 ± 0.24	06197, 06200, 06260, 06285, 06317
PL68	14.6596	−157.8591	−5639	−80 ± 12	1.17 ± 0.44	06136, 06223, 06272, 06285, 06317
PL70	15.5734	−158.9809	−5591	88 ± 7	0.77 ± 0.21	06136, 06198, 06317, 06335

time and average station delay time, but the station delay times likely reflect the structure throughout the upper mantle, whereas splitting may be dominated by shallower mantle structure. We note that the largest splitting (2.2 s) occurs at station PL44, which is a station located off of the Hawaiian Swell and has a fast station delay time. Either the fossil lithosphere has unusually strong anisotropic

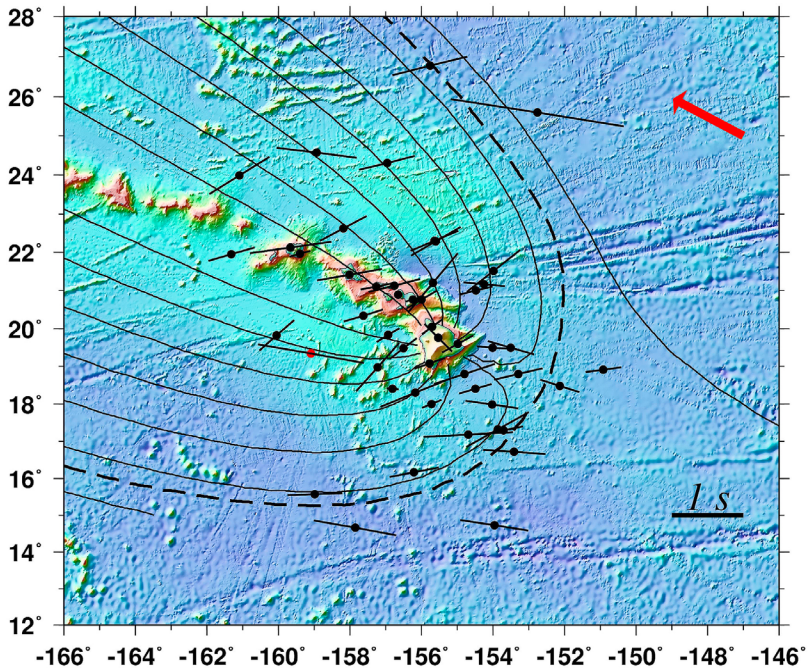

Figure 8. PLUME splitting measurements superimposed on streamlines for the parabolic asthenospheric flow (PAF) model taken from *Walker et al.* [2001]. We also plot a splitting measurement (red dot) from the OSN1 deployment [*Collins et al.*, 2002]. The measured fast polarization directions appear to be dominated by lithospheric anisotropy rather than the displayed asthenospheric flow model.

fabric at this location or some form of deeper asthenospheric anisotropy also contributes to splitting.

[23] It is useful to compare our Hawaii results with splitting patterns at other hot spot regions. Only the weak Eiffel hot spot [*Walker et al.*, 2005a] shows a parabolic pattern of splitting that conforms to a simple model of plume flow and LPO development. A parabolic pattern is not obvious at the Yellowstone hot spot [*Waite et al.*, 2005], where fast directions are mostly parallel to the direction of absolute plate motion (APM), nor at hot spots of French Polynesia [*Fontaine et al.*, 2007], where fast directions are also dominantly parallel to APM; however, seismometer spacing in the French Polynesia study may not be dense enough to detect parabolic plume flow. Splitting at the Galápagos hot spot [*Fontaine et al.*, 2005] shows a rapid change of fast directions parallel to APM to a region of no measurable anisotropy. Splitting at the Iceland hot spot [*Bjarnason et al.*, 2002; *Xue and Allen*, 2005] may be complicated by channeling of flow down the spreading ridge: alternatively, *Li and Detrick* [2003] compare surface wave azimuthal anisotropy with splitting, and suggest that splitting may be dominated by the deep background mantle flow below 100 km depth.

[24] Hawaii is the archetypal hot spot and has been estimated to have the largest buoyancy flux of any possible mantle plume [*Davies*, 1988; *Sleep*, 1990]. The lack of a parabolic splitting pattern at Hawaii does not negate the possible existence of athenospheric plume flow. But the signature of plume flow in shear wave splitting may be more subtle than previously realized, due to the presence of fossil lithospheric anisotropy and because of vertical complexities in the flow itself or complexities in the mapping between mantle deformation and LPO.

6. Conclusions

[25] Using a multiple-event method, we measure shear wave splitting at 49 land and ocean bottom seismometer stations deployed across the Hawaiian Swell during the PLUME project. Most splitting fast directions are parallel to the fossil spreading direction, and only one station yields a fast direction parallel to the direction of absolute plate motion. We suggest that splitting around Hawaii dominantly reflects the fossil lithospheric anisotropy. The signature of asthenospheric splitting is more subtle, and splitting around Hawaii thus seems to provide less direct information on plume flow, although further geodynamic modeling and

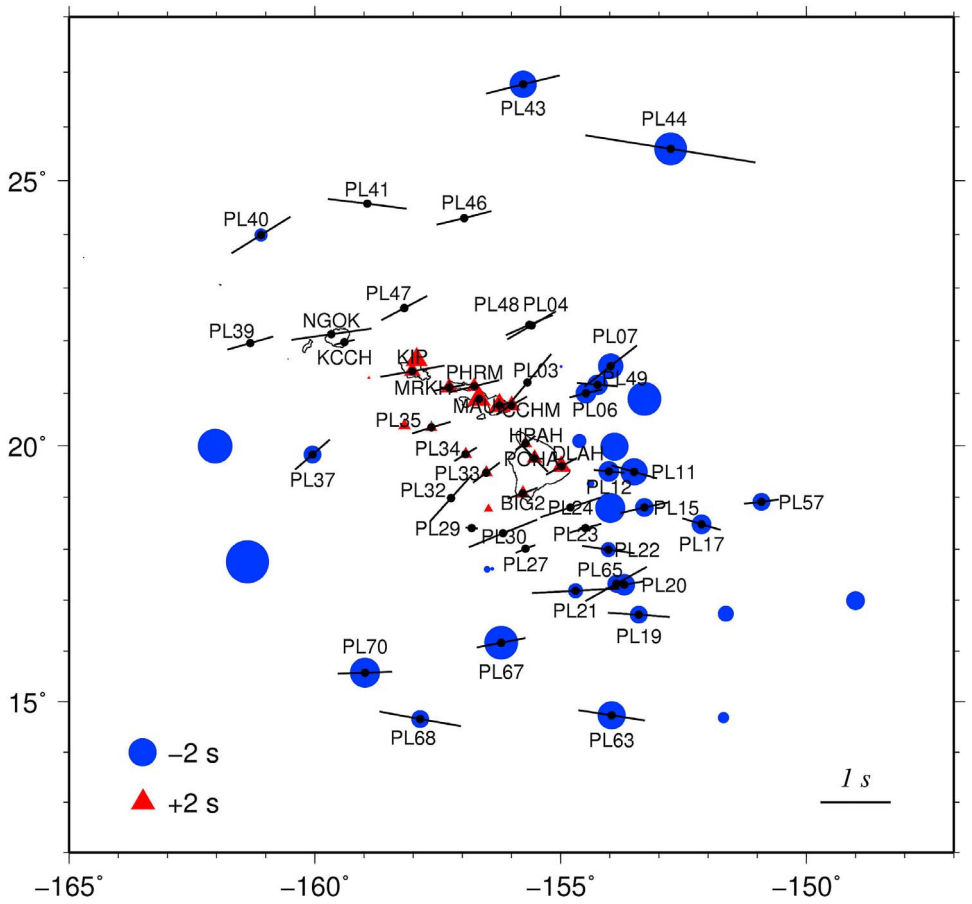

Figure 9. Map of splitting superimposed on the mean *S* wave station delays from *Wolfe et al.* [2009]. Early arrivals are shown by blue circles and late arrivals by red triangles, with symbol size scaled linearly to the magnitude of the delay (see scale at lower left). Station names are also displayed.

integration with information from surface wave anisotropy may yield additional insight. The measured splitting delay times are typically 1 s or less, although a few stations display larger splitting times of 1–2 s. There is also noticeable variability in the splitting delay times across the different stations spanning the Hawaiian Islands and Swell. We postulate that locations displaying small splitting times may have experienced processes that have altered the lithosphere and partially erased the fossil lithospheric anisotropy; alternatively, asthenospheric splitting may either constructively or destructively contribute to the lithospheric splitting, generating variability in delay times.

Acknowledgments

[26] The PLUME project was supported by NSF. We also acknowledge the crews of the research vessels Melville, Ka'imikai-O-Kanaloa, and Kilo Moana; the Jason remotely operated vehicle team; the U.S. National Ocean Bottom Seismograph Instrument Pool; the Carnegie Institution's portable seismology laboratory; and the hosts of temporary stations on the Hawaiian Islands. We thank Garrett Ito for comments on an initial version of this paper, and we appreciate the constructive comments of Thorsten Becker, Georg Rümpker, and an anonymous reviewer.

References

Abt, D. L., and K. M. Fischer (2008), Resolving three-dimensional anisotropic structure with shear wave splitting tomography, *Geophys. J. Int.*, *173*, 859–886, doi:10.1111/j.1365-246X.2008.03757.x.

Asaadi, N., N. M. Ribe, and F. Sobouti (2011), Inferring nonlinear mantle rheology from the shape of the Hawaiian swell, *Nature*, *473*, 501–504, doi:10.1038/nature09993.

Ballmer, M. D., G. Ito, J. van Hunen, and P. J. Tackley (2011), Spatial and temporal variability in Hawaiian hotspot volcanism induced by small-scale convection, *Nat. Geosci.*, *4*, 457–460, doi:10.1038/ngeo1187.

Becker, T. W., V. Schulte-Pelkum, D. K. Blackman, J. B. Kellogg, and R. J. O'Connell (2006), Mantle flow under the western United States from shear wave splitting, *Earth Planet. Sci. Lett.*, *247*, 235–251, doi:10.1016/j.epsl.2006.05.010.

Bjarnason, I. T., P. G. Silver, G. Rümpker, and S. C. Solomon (2002), Shear wave splitting across the Iceland hot spot: Results from the ICEMELT experiment, *J. Geophys. Res.*, *107*(B12), 2382, doi:10.1029/2001JB000916.

Blackman, D. K., and J.-M. Kendall (1997), Sensitivity of teleseismic body waves to mineral texture and melt in the mantle beneath a mid-ocean ridge, *Philos. Trans. R. Soc. London, Ser. A*, *355*, 217–231, doi:10.1098/rsta.1997.0007.

Blackman, D. K., and J.-M. Kendall (2002), Seismic anisotropy in the upper mantle: 2. Predictions for current plate boundary flow models, *Geochem. Geophys. Geosyst.*, *3*(9), 8602, doi:10.1029/2001GC000247.

Chevrot, S. (2006), Finite-frequency vectorial tomography: A new method for high-resolution imaging of upper mantle anisotropy, *Geophys. J. Int.*, *165*, 641–657, doi:10.1111/j.1365-246X.2006.02982.x.

Chojnacki, P., G. Laske, J. A. Orcutt, C. J. Wolfe, J. A. Collins, S. C. Solomon, R. S. Detrick, D. Bercovici, E. H. Hauri (2009), Rayleigh wave azimuthal anisotropy observed during the Hawaiian PLUME project, *Eos Trans. AGU*, *90*(52), Fall Meet. Suppl., abstract S11A-1687.

Christensen, N. I. (1984), The magnitude, symmetry and origin of upper mantle anisotropy based on fabric analyses of ultramafic tectonites, *Geophys. J. R. Astron. Soc.*, *76*, 89–111.

Collins, J. A., F. L. Vernon, J. A. Orcutt, and R. A. Stephen (2001), Broadband seismology in the oceans: Lessons from the ocean seismic network pilot experiment, *Geophys. Res. Lett.*, *28*, 49–52, doi:10.1029/2000GL011638.

Collins, J. A., F. L. Vernon, J. A. Orcutt, R. A. Stephen (2002), Upper mantle structure beneath the Hawaiian swell: Constraints from the ocean seismic network pilot experiment, *Geophys. Res. Lett.*, *29*(11), 1522, doi:10.1029/2001GL013302.

Crough, S. T. (1978), Thermal origin of mid-plate hot-spot swells, *Geophys. J. R. Astron. Soc.*, *55*, 451–469.

Davies, G. F. (1988), Ocean bathymetry and mantle convection: 1. Large-scale flow and hotspots, *J. Geophys. Res.*, *93*, 10,467–10,480, doi:10.1029/JB093iB09p10467.

Dietz, R. S., and H. W. Menard (1953), Hawaiian swell, deep and arch and subsidence of the Hawaiian Islands, *J. Geol.*, *61*, 99–113, doi:10.1086/626059.

Duennebier, F. K., D. W. Harris, J. Jolly, J. Babinec, D. Copson, and K. Stiffel (2002), underwThe Hawaii-2 Observatory seismic system, *IEEE J. Ocean Eng.*, *27*, 212–217, doi:10.1109/JOE.2002.1002475.

Duncan, R. A., and R. A. Keller (2004), Radiometric ages for basement rocks from the Emperor Seamounts, ODP leg 197, *Geochem. Geophys. Geosyst.*, *5*, Q08L03, doi:10.1029/2004GC000704.

Ekström, G., and A. M. Dziewoński (1998), The unique anisotropy of the Pacific upper mantle, *Nature*, *394*, 168–172, doi:10.1038/28148.

Farnetani, C. G., and A. W. Hofmann (2010), Dynamics and internal structure of the Hawaiian plume, *Earth Planet. Sci. Lett.*, *295*, 231–240, doi:10.1016/j.epsl.2010.04.005.

Fontaine, F. R., E. E. E. Hooft, P. G. Burkett, D. R. Toomey, S. C. Solomon, and P. G. Silver (2005), Shear-wave splitting beneath the Galápagos archipelago, *Geophys. Res. Lett.*, *32*, L21308, doi:10.1029/2005GL024014.

Fontaine, F. R., G. Barruol, A. Tommasi, and G. H. R. Bokelmann (2007), Upper-mantle flow beneath French Polynesia from shear wave splitting, *Geophys. J. Int.*, *170*, 1262–1288, doi:10.1111/j.1365-246X.2007.03475.x.

Gripp, A. E., and R. G. Gordon (2002), Young tracks of hotspots and current plate velocities, *Geophys. J. Int.*, *150*, 321–361, doi:10.1046/j.1365-246X.2002.01627.x.

Harmon, N., D. W. Forsyth, K. M. Fischer, and S. C. Webb (2004), Variations in shear-wave splitting in young Pacific seafloor, *Geophys. Res. Lett.*, *31*, L15609, doi:10.1029/2004GL020495.

Ito, G., R. Dunn, Y. Fu, A. Gallego, A. Li, and C. J. Wolfe (2011), Mantle flow and seismic anisotropy associated with plume-plate interaction, Abstract DI51C-07 presented at 2011 Fall Meeting, AGU, San Francisco, Calif., 5–9 Dec.

Jousselin, D., and D. Mainprice (1998), Melt topology and seismic anisotropy in mantle peridotites of the Oman ophiolite, *Earth Planet. Sci. Lett.*, *164*, 553–568, doi:10.1016/S0012-821X(98)00235-0.

Kaminski, É., and N. M. Ribe (2002), Timescales for the evolution of seismic anisotropy in mantle flow, *Geochem. Geophys. Geosyst.*, *3*(8), 1051, doi:10.1029/2001GC000222.

Karato, S. (2008), Insight into the plume-upper mantle interaction inferred from the central Pacific geophysical anomalies, *Earth Planet. Sci. Lett.*, *274*, 234–240, doi:10.1016/j.epsl.2008.07.033.

Karato, S., H. Jung, I. Katayama, and P. A. Skemer (2008), Geodynamic significance of seismic anisotropy of the upper mantle: New insights from laboratory studies, *Annu. Rev. Earth Planet. Sci.*, *36*, 59–95, doi:10.1146/annurev.earth.36.031207.124120.

Laske, G., J. A. Collins, C. J. Wolfe, S. C. Solomon, R. S. Detrick, J. A. Orcutt, D. Bercovici, and E. H. Hauri (2009), Probing the Hawaiian hot spot with new broadband ocean bottom instruments, *Eos Trans. AGU*, *90*(41), 362, doi:10.1029/2009EO410002.

Laske, G., A. Markee, J. A. Orcutt, C. J. Wolfe, J. A. Collins, S. C. Solomon, R. S. Detrick, D. Bercovici, and E. H. Hauri (2011), Asymmetric shallow mantle structure beneath the Hawaiian Swell–Evidence from Rayleigh waves recorded by the PLUME network, *Geophys. J. Int.*, *187*, 1725–1742, doi:10.1111/j.1365-246X.2011.05238.x.

Leahy, G. M., J. A. Collins, C. J. Wolfe, G. Laske, and S. C. Solomon (2010), Magmatic underplating of the Hawaiian Swell, *Geophys. J. Int.*, *183*, 313–329, doi:10.1111/j.1365-246X.2010.04720.x.

Li, A., and R. S. Detrick (2003), Azimuthal anisotropy and phase velocity beneath Iceland: Implications for plume-ridge interaction, *Earth Planet. Sci. Lett.*, *214*, 153–165, doi:10.1016/S0012-821X(03)00382-0.

Mainprice, D., and P. G. Silver (1993), Interpretation of *SKS* waves using samples from the subcontinental lithosphere, *Phys. Earth Planet. Inter.*, *78*, 257–280, doi:10.1016/0031-9201(93)90160-B.

Marone, F., and B. Romanowicz (2007), The depth distribution of azimuthal anisotropy in the continental mantle, *Nature*, *447*, 198–201, doi:10.1038/nature05742.

Monteiller, V., and S. Chevrot (2010), How to make robust splitting measurements for single-station analyses and three-dimensional imaging of seismic anisotropy, *Geophys. J. Int.*, *182*, 311–328.

Moore, W. B., G. Schubert, and P. Tackley (1998), Three-dimensional simulations of plume-lithosphere interaction at the Hawaiian swell, *Science*, *279*, 1008–1011, doi:10.1126/science.279.5353.1008.

Morgan, W. J. (1971), Convection plumes in the lower mantle, *Nature*, *230*, 42–43, doi:10.1038/230042a0.

Müller, R. D., W. R. Roest, J.-Y. Royer, L. M. Gahagan, and J. G. Sclater (1997), Digital isochrones of the world's ocean floor, *J. Geophys. Res.*, *102*, 3211–3214, doi:10.1029/96JB01781.

Nettles, M., and A. M. Dziewoński (2008), Radially anisotropic shear velocity structure of the upper mantle globally and beneath North America, *J. Geophys. Res.*, *113*, B02303, doi:10.1029/2006JB004819.

Nishimura, C. E., and D. W. Forsyth (1988), Rayleigh wave phase velocities in the Pacific with implications for azimuthal anisotropy and lateral heterogeneities, *Geophys. J. R. Astron. Soc.*, *94*, 479–501.

Nishimura, C. E., and D. W. Forsyth (1989), The anisotropic structure of upper mantle in the Pacific, *Geophys. J.*, *96*, 203–229, doi:10.1111/j.1365-246X.1989.tb04446.x.

Restivo, A., and G. Helffrich (1999), Teleseismic shear wave splitting measurements in noisy environments, *Geophys. J. Int.*, *137*, 821–830, doi:10.1046/j.1365-246x.1999.00845.x.

Ribe, N. M., and U. R. Christensen (1999), The dynamical origin of Hawaiian volcanism, *Earth Planet. Sci. Lett.*, *171*, 517–531, doi:10.1016/S0012-821X(99)00179-X.

Rümpker, G., and P. G. Silver (1998), Apparent shear-wave splitting parameters in the presence of vertically varying anisotropy, *Geophys. J. Int.*, *135*, 790–800, doi:10.1046/j.1365-246X.1998.00660.x.

Rümpker, G., and P. G. Silver (2000), Calculating splitting parameters for plume-type anisotropic structures of the upper mantle, *Geophys. J. Int.*, *143*, 507–520, doi:10.1046/j.1365-246X.2000.00056.x.

Saltzer, R. L., J. B. Gaherty, and T. H. Jordan (2000), How are vertical shear wave splitting measurements affected by variations in the orientation of azimuthal anisotropy with depth?, *Geophys. J. Int.*, *141*, 374–390, doi:10.1046/j.1365-246x.2000.00088.x.

Searle, R., R. T. Holcomb, J. B. Wilson, M. L. Holmes, R. J. Whittington, E. S. Kappel, B. A. McGregor, and A. N. Shor (1993), The Molokai Fracture Zone near Hawaii, and the Late Cretaceous change in Pacific/Farallon spreading direction, in *The Mesozoic Pacific: Geology, Tectonics, and Volcanism: A Volume in Memory of Sy Schlanger*, *Geophys. Monogr. Ser.*, vol. 77, edited by M. S. Pringle et al., pp. 155–169, AGU, Washington, D. C., doi:10.1029/GM077p0155.

Silver, P. G., and W. W. Chan (1991), Shear-wave splitting and subcontinental mantle deformation, *J. Geophys. Res.*, *96*, 16,429–16,454, doi:10.1029/91JB00899.

Silver, P. G., and M. K. Savage (1994), The interpretation of shear-wave splitting parameters in the presence of two anisotropic layers, *Geophys. J. Int.*, *119*, 949–963, doi:10.1111/j.1365-246X.1994.tb04027.x.

Silver, P. G., D. Mainprice, W. Ben Ismaïl, A. Tommasi, and G. Barruol (1999), Mantle structural geology from seismic anisotropy, in *Mantle Petrology: Field Observations and High Pressure Experimentations: A Tribute to Francis R. (Joe) Boyd*, edited by Y. Fei, C. M. Bertka, and B. O. Mysen, *Spec. Publ. Geochem. Soc.*, 6, 79–103.

Sleep, N. H. (1990), Hotspots and mantle plumes: Some phenomenology, *J. Geophys. Res.*, *95*, 6715–6736, doi:10.1029/JB095iB05p06715.

Smith, W. H. F., and D. T. Sandwell (1997), Global seafloor topography from satellite altimetry and ship depth soundings, *Science*, *277*, 1956–1962, doi:10.1126/science.277.5334.1956.

Sobolev, A. V., A. W. Hofmann, S. V. Sobolev, and I. K. Nikogosian (2005), An olivine-free mantle source of Hawaiian shield basalts, *Nature*, *434*, 590–597, doi:10.1038/nature03411.

Van Ark, E., and J. Lin (2004), Time variation in igneous volume flux of the Hawaiian-Emporer hot spot seamount chain, *J. Geophys. Res.*, *109*, B11401, doi:10.1029/2003JB002949.

Waite, G. P., D. L. Schutt, and R. B. Smith (2005), Models of lithosphere and asthenosphere anisotropic structure of the Yellowstone hotspot from shear wave splitting, *J. Geophys. Res.*, *110*, B11304, doi:10.1029/2004JB003501.

Walker, K. T., G. H. R. Bokelmann, and S. L. Klemperer (2001), Shear-wave splitting to test mantle deformation models around Hawaii, *Geophys. Res. Lett.*, *28*, 4319–4322, doi:10.1029/2001GL013299.

Walker, K. T., G. H. R. Bokelmann, and S. L. Klemperer (2003), Reply to "Shear-wave splitting to test mantle deformation around Hawaii" by Vinnik et al., *Geophys. Res. Lett.*, *30*(13), 1676, doi:10.1029/2002GL016712.

Walker, K. T., G. H. R. Bokelmann, S. L. Klemperer, and G. Bock (2005a), Shear-wave splitting around the Eifel hotspot: Evidence for a mantle upwelling, *Geophys. J. Int.*, *163*, 962–980, doi:10.1111/j.1365-246X.2005a.02636.x.

Walker, K. T., G. H. R. Bokelmann, S. L. Klemperer, and A. Nyblade (2005b), Shear wave splitting around hotspots: Evidence for upwelling-related mantle flow?, *Spec. Pap. Geol. Soc. Am.*, *288*, 171–192.

Watts, A. B., U. S. ten Brink, P. Buhl, and T. M. Brocher (1985), A multichannel seismic study of lithospheric flexure across the Hawaiian-Emperor seamount chain, *Nature*, *315*, 105–111, doi:10.1038/315105a0.

Wolfe, C. J., and P. G. Silver (1998), Seismic anisotropy of oceanic upper mantle: Shear-wave splitting methodologies and observations, *J. Geophys. Res.*, *103*, 749–771, doi:10.1029/97JB02023.

Wolfe, C. J., and S. C. Solomon (1998), Shear-wave splitting and implications for mantle flow beneath the MELT region of the East Pacific Rise, *Science*, *280*, 1230–1232, doi:10.1126/science.280.5367.1230.

Wolfe, C. J., P. G. Okubo, G. Ekström, M. Nettles, and P. M. Shearer (2004), Characteristics of deep (<13 km) Hawaiian earthquakes and Hawaiian earthquakes west of 155.55°W, *Geochem. Geophys. Geosyst.*, *5*, Q04006, doi:10.1029/2003GC000618.

Wolfe, C. J., S. C. Solomon, G. Laske, J. A. Collins, R. S. Detrick, J. A. Orcutt, D. Bercovici, and E. H. Hauri (2009), Mantle shear-wave velocity structure beneath the Hawaiian hot spot, *Science*, *326*, 1388–1390, doi:10.1126/science.1180165.

Wolfe, C. J., S. C. Solomon, G. Laske, J. A. Collins, R. S. Detrick, J. A. Orcutt, D. Bercovici, and E. H. Hauri (2011), Mantle *P*-wave velocity structure beneath the Hawaiian hot spot, *Earth Planet. Sci. Lett.*, *303*, 267–280, doi:10.1016/j.epsl.2011.01.004.

Xue, M., and R. M. Allen (2005), Asthenospheric channeling of the Iceland upwelling: Evidence from seismic anisotropy, *Earth Planet. Sci. Lett.*, *235*, 167–182, doi:10.1016/j.epsl.2005.03.017.

Zhang, S., and S.-i. Karato (1995), Lattice preferred orientation of olivine aggregates deformed in simple shear, *Nature*, *375*, 774–777, doi:10.1038/375774a0.